Density-functional theory for the freezing of Stockmayer fluids

B. Groh and S. Dietrich
Fachbereich Physik, Bergische Universität Wuppertal, D-42097 Wuppertal, Federal Republic of Germany
(Received 16 April 1996)

We examine the freezing of Stockmayer fluids which consist of spherical particles interacting via Lennard-Jones and dipolar forces and thus represent, e.g., models for ferrofluids. The theoretical analysis is based on an appropiate version of density-functional theory which is capable of describing both the freezing transition and the formation of orientationally ordered phases. This allows us to study the variation of the topology of phase diagrams as a function of the strength of the dipole moment of the particles. We find an isotropic gas and liquid phase, a ferromagnetic liquid, an orientationally disordered solid, and a ferromagnetic solid. For small dipole moments the formation of the ferromagnetic liquid is preempted by freezing. For the ferromagnetic solid the face-centered-cubic structure turns out to be more stable than the body-centered-tetragonal structure. [S1063-651X(96)09108-8]

PACS number(s): 64.70.Dv, 75.50.Mm, 75.30.Kz, 77.80.−e

I. INTRODUCTION

There is mounting theoretical evidence that *spherical* particles endowed with an anisotropic interaction potential can form a *fluid* phase with long-ranged orientational order. This ferromagnetic nematic phase has been observed in a number of Monte Carlo simulations for dipolar soft [1,2] and hard [3–5] spheres as well as for the Stockmayer fluid [6], which consists of spherical particles which possess a pointlike permanent dipole moment and in addition interact according to the spherically symmetric Lennard-Jones potential. These findings have been confirmed and analyzed systematically within the framework of density-functional theory [7–9] which refines more phenomenological descriptions [10–13]. Similar phase diagrams have been reported [14–17] for so-called Heisenberg fluids [18–21] whose particles have an anisotropic interaction due to a *short-ranged* Heisenberg exchange coupling between fixed spins. If instead the Lennard-Jones part of the interaction potential is augmented by a nonspherically symmetric contribution of the same range exhibiting an angular modulation which varies twice as rapidly as the dipole-dipole interaction potential, one observes the formation of a nonferromagnetic nematic phase [22–24].

For three reasons the Stockmayer fluid with its *long-ranged* dipolar interaction is particularly interesting. First, it represents a reasonable model for molecular fluids whose constituents carry a permanent electric dipole moment. Second, it can also be used as an effective model for ferrofluids which are colloidal suspensions of permanently magnetized spherical particles. Third, due to the slow decay of the dipolar interaction the type of long-ranged orientationally order differs from the parallel alignment known of ferromagnets with short-ranged exchange interaction. One finds that the actual configuration displays a smooth spatial variation on the scale of the size of the sample [25]. These domains are not pinned by lattice anisotropies or lattice imperfections as they occur in solid ferromagnets with dipolar interactions. It is this particular kind of inhomogeneous magnetization structure which yields a free energy which does not depend on the sample shape in spite of shape-dependent demagnetization effects [26,27,25].

It turns out that such an orientationally ordered liquid phase appears at high number densities. Since in the analytic calculations so far the freezing of the liquid has not been considered and the Monte Carlo calculations cannot sweep the full phase space spanned by the thermodynamic variables and the interaction parameters of the model, one faces the important question of whether the freezing of the fluid preempts the formation of a liquid phase with long-ranged orientational order. To this end we study a density-functional theory which is able to address this question.

In the past decade density-functional theories have evolved which offer a unified and quantitatively reliable description of the vapor, liquid, and solid phases of classical fluids. A number of sophisticated approaches have been designed in order to analyze the liquid-solid phase transition as well as the equilibrium structure of the solid based on liquid state correlation functions [28]. These theories have mainly been tested for the simplest model which exhibits a freezing transition, i.e., the hard-sphere system. In general the results are in fair agreement with Monte Carlo simulation data. If the liquid state correlation functions required as an input are obtained from numerical simulations or from integral equation theories such as the hypernetted-chain approximation, these density-functional theories can be generalized to fluids with long-ranged attractive interactions. In another approach the attractive interactions are treated as a perturbation of the hard-sphere system and are included as a mean-field-like correction in the density functional. One successful example for such an approach has been given by Curtin and Ashcroft [29], who obtained a phase diagram for the Lennard-Jones system in good agreement with numerical simulations.

The freezing of anisotropic particles has been tackled only in a few cases for fluids of hard ellipsoids [30–33], hard dumbbells [30,33,34], and dipolar hard spheres [33,35]. The reason for the much higher complexity of this problem compared to atomic fluids lies in the increased number of variables entering the interaction potential and the correlation functions as well as in the large variety of conceivable crystal structures due to the lower symmetry in the case of orientational order in the solid. Nonetheless, in order to address the question formulated above we undertake the difficult task

of constructing a density-functional theory for the freezing of the Stockmayer fluid. For reasons of simplicity we shall only consider two possible lattice structures: the fcc lattice, which is known to be stable for the Lennard-Jones fluid and therefore may be expected to remain so at least for small dipole moments, and the body-centered-tetragonal (bct) lattice, which has been observed in simulations [2,4] and in experiments with electrorheological fluids [36] in which the induced dipole moments of colloidal particles are forced to point in the direction fixed by an external electrical field.

We are aware of only two previous studies [35,33] in which density-functional theory has been applied to the freezing of dipolar fluids. Both of them use the perturbative density-functional approach initiated by Ramakrishnan and Yussouff [37] in connection with the direct correlation function given by first-order perturbation theory. However, the results of McMullen and Oxtoby [35] have been invalidated by an Erratum [38]. Smithline *et al.* [33] do not find an orientationally ordered crystal, but their approach suffers from an incorrect treatment of the long-ranged dipolar interaction (see below, end of Sec. III). Thus the present work can be regarded as a first step towards a liquid-based theory of dipolar solids. Future steps should focus on improving the quantitative reliability of this approach.

II. DENSITY-FUNCTIONAL THEORY

The Stockmayer fluid consists of spherically symmetric particles, interacting via the Lennard-Jones potential,

$$w_{\mathrm{LJ}}(r_{12})=4\epsilon\left[\left(\frac{\sigma}{r_{12}}\right)^{12}-\left(\frac{\sigma}{r_{12}}\right)^{6}\right], \tag{2.1}$$

with embedded point dipoles which give rise to the dipolar interaction potential

$$w_{\mathrm{dip}}(\mathbf{r}_{12},\omega,\omega')=-\frac{m^2}{r_{12}^3}\left(\frac{3[\hat{\mathbf{m}}(\omega)\cdot\mathbf{r}_{12}][\hat{\mathbf{m}}(\omega')\cdot\mathbf{r}_{12}]}{r_{12}^{\,2}}-\hat{\mathbf{m}}(\omega)\cdot\hat{\mathbf{m}}(\omega')\right)\Theta(r_{12}-\sigma) \tag{2.2}$$

with $\mathbf{r}_{12}=\mathbf{r}-\mathbf{r}'$, where $\mathbf{r}$ and $\mathbf{r}'$ denote the positions of the interacting particles and ω and ω' their orientations. $\hat{\mathbf{m}}$ is a unit vector in the direction of ω and m the absolute value of the dipole moment. The dipolar potential is cut off for particle separations less than σ. Within the framework of density-functional theory the system is described by the number density of particles at a point $\mathbf{r}$ and with orientation ω:

$$\hat{\rho}(\mathbf{r},\omega)=\rho(\mathbf{r})\,\alpha(\mathbf{r},\omega). \tag{2.3}$$

The angular distribution $\alpha(\mathbf{r},\omega)$ is normalized to 1 so that $\rho_0=1/V\int_V d^3r\,\rho(\mathbf{r})$ is the overall mean density of the sample with volume V.

In order to construct a density-functional theory which describes both the fluid and the solid phases of the Stockmayer system, we generalize our ansatz of Refs. [8,9]. Within this approach the interaction potential is separated into a suitable short-ranged reference part and a long-ranged part which is treated perturbatively. The reference system is approximated by a hard-sphere fluid with a temperature dependent hard-sphere diameter given by the Barker-Henderson formula [39] [$\beta=(k_BT)^{-1}$]

$$d(T)=\int_0^{\sigma}dr\,(1-e^{-\beta w_{\mathrm{LJ}}(r)}). \tag{2.4}$$

Due to the strong spatial variations of the density on the length scale of the particle diameter, as it occurs in the solid phase, the simple local-density approximation used in Refs. [8,9] for the free energy of the reference system has to be replaced by a more sophisticated version. Out of the large number of possibilities which have been suggested in the literature (for reviews see Refs. [28,40,41]) we choose the modified weighted density approximation (MWDA) [42]. This approach is relatively simple from the computational point of view because it is based on a globally weighted density $\overline{\rho}$ obtained from an appropriate average of the actual density distribution in the solid. On the other hand, this prevents its application to the description of interfacial phenomena. Nevertheless the MWDA yields satisfactory results for the fluid-solid transition of hard spheres so that we adopt this scheme for the description of the reference system. Within this approximation the reference contribution to the total free energy $F=F_{\mathrm{ref}}+F_{\mathrm{exc}}$ is

$$F_{\mathrm{ref}}[\{\hat{\rho}(\mathbf{r},\omega)\}]=\frac{1}{\beta}\int_V d^3r\,\rho(\mathbf{r})[\ln(\rho(\mathbf{r})\lambda^3)-1]+\frac{1}{\beta}\int_V d^3r\int d\omega\,\hat{\rho}(\mathbf{r},\omega)\ln(4\pi\alpha(\mathbf{r},\omega))+V\rho_0 f_{\mathrm{PY}}(\overline{\rho}), \tag{2.5}$$

where the first two terms represent the ideal gas contribution with the thermal wavelength λ. The second term vanishes in the case of an isotropic orientational distribution for which $\alpha(\mathbf{r},\omega)=1/(4\pi)$. The last term is the Percus-Yevick free energy of the hard-sphere fluid evaluated at the weighted density $\overline{\rho}$:

$$\beta f_{\mathrm{PY}}(\overline{\rho})=\frac{3}{2}\left(\frac{1}{(1-\eta)^2}-1\right)-\ln(1-\eta) \tag{2.6}$$

with the packing fraction $\eta=(\pi/6)d(T)^3\overline{\rho}$. The weighted density $\overline{\rho}$ is given implicitly by

$$\overline{\rho}=\frac{1}{\rho_0 V}\int_V d^3r\int_V d^3r'\,\rho(\mathbf{r})\rho(\mathbf{r}')\overline{w}(\mathbf{r}_{12};\overline{\rho}), \tag{2.7}$$

where the weighting function $\overline{w}$ is determined by the requirement that in the limit of a homogeneous fluid the second functional derivative of the free energy yields the Percus-Yevick direct correlation function:

$$-\beta\lim_{\rho(\mathbf{r})\to\rho_0}\frac{\delta^2[V\rho_0 f_{\mathrm{PY}}(\overline{\rho})]}{\delta\rho(\mathbf{r})\,\delta\rho(\mathbf{r}')}=c_{\mathrm{PY}}(\mathbf{r}-\mathbf{r}';\rho_0). \tag{2.8}$$

If the density distribution in the solid is parametrized as a sum of Gaussian distributions of width γ centered at the lattice points $\mathbf{R}$,

$$\rho(\mathbf{r})=\left(\frac{\gamma}{\pi}\right)^{3/2}\sum_{\mathbf{R}} e^{-\gamma(\mathbf{r}-\mathbf{R})^2}, \tag{2.9}$$

Eq. (2.8) yields in the thermodynamic limit the following implicit equation for $\overline{\rho}$ [42],

$$\overline{\rho}(\rho_0,\gamma)=\rho_0\left(1-\frac{1}{2\beta f'_{\mathrm{PY}}(\overline{\rho})}\sum_{\mathbf{q}\neq 0} e^{-q^2/2\gamma}c_{\mathrm{PY}}(q;\overline{\rho})\right), \tag{2.10}$$

in which the sum runs over the corresponding reciprocal lattice vectors and $c_{\mathrm{PY}}(q;\overline{\rho})$ is the Fourier transform of the direct correlation function. (For an fcc crystal of hard spheres this equation has actually two solutions [43], one of which is larger than ρ_0 and is therefore discarded for physical reasons.) In Eq. (2.9) and in the following the lattice sum over $\mathbf{R}$ is unlimited and its truncation for a finite volume V is accomplished by restricting the integrations over $\mathbf{r}$ and $\mathbf{r}'$, respectively, to the sample volume V.

In agreement with Refs. [42] and [29] we use the Carnahan-Starling formula [44]

$$\beta f_{\mathrm{CS}}=\eta\frac{4-3\eta}{(1-\eta)^2} \tag{2.11}$$

for the *fluid* phases which renders better results for high densities, at which the liquid-solid transition takes place. [This construction leads to a discontinuity of the density-functional upon approaching a homogeneous configuration $\rho(\mathbf{r})=\rho_0$ from a periodically varying solid configuration with the same mean density. However, this does not pose a problem, because this discontinuity is not reached due to the density gap of the first-order liquid-solid transitions. Moreover, using the Percus-Yevick approximation also for the liquid, which would be more appealing from a principal point of view, results only in a slight modification of the coexistence densities of hard spheres [41].]

In order to limit the number of minimization parameters we consider only density configurations which fulfill the following requirements.

(i) The spatial and orientational dependences factorize, i.e., $\hat{\rho}(\mathbf{r},\omega)=\rho(\mathbf{r})\alpha(\omega)$. We focus on the case of a vanishing demagnetization factor (i.e., a long and thin sample), for which the above factorization is fulfilled in the ferromagnetic liquid [25]. We expect that this is a reasonable approximation also for the solid.

(ii) The solid has an fcc structure, which is known to be true for the Lennard-Jones fluid. We assume that the direction of the magnetization is parallel to the long axis of the sample. However, the orientation of the lattice relative to this axis is left for minimization. This addresses the issue of the most favorable lattice orientation of the solid which emerges from an orientationally ordered liquid by freezing. As it will turn out, this orientation is determined by *bulk* contributions to the free energy [see below the discussion following Eq. (3.36)].

(iii) The orientational distribution has axial symmetry, i.e.,

$$\alpha(\omega)=\frac{1}{2\pi}\sum_{l=0}^{\infty}\alpha_l P_l(\cos\theta), \tag{2.12}$$

where P_l are Legendre polynomials and θ denotes the angle with respect to the preferred direction $\hat{\mathbf{M}}$. This symmetry does hold in a liquid. If there are deviations in a solid they must be compatible with the symmetry of the lattice. Therefore, in a more general expansion of the orientational distribution in terms of spherical harmonics $Y_{lm}(\omega)$, contributions with $m\neq 0$ may arise only for rather large values of l, e.g., for $l\geq 3$ if $\hat{\mathbf{M}}\|\langle 111\rangle$ and for $l\geq 4$ if $\hat{\mathbf{M}}\|\langle 100\rangle$, where $\langle lhk\rangle$ is the standard notation for a set of equivalent lattice direction.

(iv) Following the literature we parametrize the number density according to Eq. (2.9). For hard spheres a more general ansatz in terms of a Fourier series as well as Monte Carlo simulations have revealed only small deviations from this form [41].

For sharp peaks with small overlap, i.e., for large values of γ, and in the thermodynamic limit Eq. (2.9) leads to the following approximate expression for the translational entropy contribution in Eq. (2.5):

$$\begin{aligned}\int_V d^3r\,\rho(\mathbf{r})\ln(\rho(\mathbf{r})\lambda^3)&=\left(\frac{\gamma}{\pi}\right)^{3/2}\sum_{\mathbf{R}}\int_V d^3r\, e^{-\gamma(\mathbf{r}-\mathbf{R})^2}\\&\quad\times\left\{\ln\left[\left(\frac{\gamma}{\pi}\right)^{3/2}\lambda^3\right]-\gamma(\mathbf{r}-\mathbf{R})^2\right\}\\&\quad+O(e^{-4\gamma R_1^2})\\&=\rho_0 V\left[\frac{3}{2}\ln(\lambda^2\gamma/\pi)-\frac{3}{2}\right]\\&\quad+O(e^{-4\gamma R_1^2}),\end{aligned} \tag{2.13}$$

where $2R_1$ is the nearest neighbor distance in the lattice.

III. EXCESS CONTRIBUTION TO THE DENSITY FUNCTIONAL

A. Ansatz for the excess free energy

Regarding the perturbative contribution to the free energy stemming from the excess part of the interaction potential, one could be inclined to adopt from Refs. [8,9,25] the expression

$$\begin{aligned}F_{\mathrm{exc}}^{\mathrm{app}}=&-\frac{1}{2\beta}\int_V d^3r\int_V d^3r'\,d\omega\,d\omega'\,\hat{\rho}(\mathbf{r},\omega)\hat{\rho}(\mathbf{r}',\omega')\\&\times\Theta(r_{12}-\sigma)\tilde{f}(\mathbf{r}-\mathbf{r}',\omega,\omega')\end{aligned} \tag{3.1}$$

with

$$\tilde{f}(\mathbf{r}_{12},\omega,\omega')=(e^{-\beta[w_{\mathrm{LJ}}(r_{12})+w_{\mathrm{dip}}(\mathbf{r}_{12},\omega,\omega')]}-1). \tag{3.2}$$

But this leads to unreasonable results already for the pure Lennard-Jones fluid (e.g., at $T^*=k_BT/\epsilon=1.35$ the values of the liquid and solid densities at coexistence are $\rho_l^*=\rho_l\sigma^3=0.89$ and $\rho_s^*=\rho_s\sigma^3=1.35$ as compared with $\rho_l^*=0.964$ and $\rho_s^*=1.053$ from numerical simulations [45]). Therefore we combine Eq. (3.1) with the ansatz of Curtin and Ashcroft [29] which for the Lennard-Jones systems

yields results that are in good agreement with simulation data. To this end the excess contribution is divided into two parts:

$$F_{\rm exc}=F_{{\rm exc},l}+\Delta F_{\rm exc}, \tag{3.3}$$

where the contribution for an isotropic fluid is approximated by

$$\frac{F_{{\rm exc},l}}{V}=\frac{1}{2}\rho_0^2\int_V d^3r\Big[g_{\rm HS}(\rho_0,r)w_{\rm LJ}(r)+\frac{1}{\beta}(1-\langle\exp(-\beta w_{\rm dip}(\mathbf{r},\omega,\omega'))\rangle_{\omega\omega'})\Big]. \tag{3.4}$$

Here $\langle\cdots\rangle_{\omega,\omega'}$ denotes the average over the molecular orientations ω and ω' and $g_{\rm HS}(\rho_0,r)$ is the Percus-Yevick pair distribution function for hard spheres [46]. For the ferromagnetic liquid as well as for the solid we add the expression

$$\Delta F_{\rm exc}=\frac{1}{2}\int_V d^3r\,d\omega\int_V d^3r'\,d\omega'\left(\hat\rho(\mathbf{r},\omega)-\frac{\rho_0}{4\pi}\right)\times\left(\hat\rho(\mathbf{r}',\omega')-\frac{\rho_0}{4\pi}\right)\widetilde{w}(\mathbf{r}-\mathbf{r}',\omega,\omega') \tag{3.5}$$

with

$$\widetilde{w}(\mathbf{r}_{12},\omega,\omega')=\begin{cases} w_{\rm LJ}(r_{12})+\dfrac{1}{\beta}[1-\exp(-\beta w_{\rm dip}(\mathbf{r}_{12},\omega,\omega'))], & r_{12}>R_2\\ -\epsilon+\dfrac{1}{\beta}[1-\exp(-\beta w_{\rm dip}(\mathbf{r}_{12},\omega,\omega'))], & \sigma<r_{12}<R_2\\ -\epsilon, & R_1<r_{12}<\sigma\\ 0, & r_{12}<R_1\end{cases}. \tag{3.6}$$

$R_2=2^{1/6}\sigma$ denotes the position of the minimum of the Lennard-Jones potential and $R_1=R_1(\rho_0)$ is half the nearest neighbor distance in the solid (for an fcc crystal $R_1=2^{-5/6}\rho_0^{-1/3}$ so that for reasonable solid densities $\rho_0\sigma^3\geqslant 0.8$ one has $R_1<\sigma$; for a ferromagnetic liquid the dependence of $\Delta F_{\rm exc}$ on R_1 drops out). The cutoff at $r_{12}=R_1$ prevents self-interaction effects [29] and is necessary to obtain a liquid-solid transition within a reasonable density range. In Eq. (3.6) the Lennard-Jones potential is not included in the argument of the exponential in order to ensure that in the absence of a dipole moment Eqs. (3.3)–(3.6) reduce to the ansatz of Curtin and Ashcroft [29].

B. Fluid and solid phases

Like any function that depends only on the relative orientations and positions of two uniaxial molecules the kernel

$$\widetilde{w}(\mathbf{r}_{12},\omega,\omega')=\sum_{l_1l_2l} w_{l_1l_2l}(r_{12})\Phi_{l_1l_2l}(\omega,\omega',\omega_{12}) \tag{3.7}$$

can be expanded in terms of the rotational invariant functions $\Phi_{l_1l_2l}$ defined as [47]

$$\Phi_{l_1l_2l}(\omega,\omega',\omega_{12})=\sum_{m_1,m_2,m} C(l_1l_2l,m_1m_2m)\times Y_{l_1m_1}(\omega)Y_{l_2m_2}(\omega')Y^*_{lm}(\omega_{12}). \tag{3.8}$$

The numbers $C(l_1l_2l,m_1m_2m)$ denote Clebsch-Gordan coefficients. In terms of these functions the dipolar potential is simply given by

$$w_{\rm dip}(\mathbf{r}_{12},\omega,\omega')=-\frac{m^2}{r_{12}^3}(4\pi)^{3/2}\sqrt{\tfrac{2}{15}}\Phi_{112}(\omega,\omega',\omega_{12}). \tag{3.9}$$

Equation (3.5) can be written as a sum of three terms:

$$\begin{aligned}\Delta F_{\rm exc}&=\frac{1}{2}\int_V d^3r\,d\omega\int_V d^3r'\,d\omega'\,\hat\rho(\mathbf{r},\omega)\hat\rho(\mathbf{r}',\omega')\times\widetilde{w}(\mathbf{r}-\mathbf{r}',\omega,\omega')\\&\quad-\frac{\rho_0}{4\pi}\int_V d^3r\,d\omega\int_V d^3r'\,d\omega'\,\hat\rho(\mathbf{r},\omega)\widetilde{w}(\mathbf{r}-\mathbf{r}',\omega,\omega')\\&\quad+\frac{1}{2}\left(\frac{\rho_0}{4\pi}\right)^2\int_V d^3r\,d\omega\int_V d^3r'\,d\omega'\,\widetilde{w}(\mathbf{r}-\mathbf{r}',\omega,\omega')\\&=\Delta F_{\rm exc}^{(1)}-2\Delta F_{\rm exc}^{(2)}+\Delta F_{\rm exc}^{(3)}\\&=\Delta F_{\rm exc}^{(SR)}+\Delta F_{\rm exc}^{(\rm LR)}.\end{aligned} \tag{3.10}$$

Here, in order to proceed, we separated the kernel $\widetilde{w}=\widetilde{w}^{\,(\rm SR)}+\widetilde{w}^{\,(\rm LR)}$ into a long-ranged part $\widetilde{w}^{\,(\rm LR)}$ decaying $\sim r_{12}^{-3}$ at large distances and a short-ranged part $\widetilde{w}^{\,(\rm SR)}$ whose contributions decay $\sim r_{12}^{-6}$ or faster. The expansion of the exponential in Eq. (3.6) shows that the long-ranged part is just the dipolar potential $w_{\rm dip}$. Terms containing this part must be treated carefully because integrals of the form

$\int_V d^3r\widetilde{w}^{(\mathrm{LR})}(\mathbf{r},\omega,\omega')$ are divergent for $V\to\infty$. On the other hand, one has $\int d\omega' w_{\mathrm{dip}}(\mathbf{r},\omega,\omega')=0$ so that the long-ranged part of $\widetilde{w}$ can be ignored in $\Delta F_{\mathrm{exc}}^{(2)}$ and $\Delta F_{\mathrm{exc}}^{(3)}$ Thus one finds in the thermodynamic limit

$$\begin{aligned}\lim_{V\to\infty}\frac{\Delta F_{\mathrm{exc}}^{(3)}}{V}&=\frac{1}{2}\frac{\rho_0^2}{(4\pi)^{1/2}}\int_{R_1}^{\infty}drr^2w_{000}(r)\\&=-2\pi\rho_0^2\epsilon(\sqrt{2}\sigma^3-R_1^3+\tfrac{5}{9}\sqrt{2}\sigma^3)\\&\quad+\frac{1}{2}\rho_0^2\int_{\mathbb{R}^3}d^3r\frac{1}{\beta}\\&\quad\times[1-\langle\exp(-\beta w_{\mathrm{dip}}(\mathbf{r},\omega,\omega'))\rangle_{\omega\omega'}].\end{aligned}\tag{3.11}$$

With the substitution $(\mathbf{r},\mathbf{r}-\mathbf{r}')=(\mathbf{r}_1,\mathbf{r}_{12})$ the second term in Eq. (3.10) can be written as

$$\begin{aligned}\lim_{V\to\infty}\frac{\Delta F_{\mathrm{exc}}^{(2)}}{V}&=\frac{1}{2}\frac{\rho_0^2}{4\pi}\int_{R_1}^{\infty}dr_{12}d\omega r_{12}^2\alpha(\omega)\\&\quad\times\left[\int d\omega_{12}d\omega'\widetilde{w}(\mathbf{r}_{12},\omega,\omega')\right].\end{aligned}\tag{3.12}$$

Using Eqs. (3.7) and (3.8) it can be shown that the expression in square brackets does not depend on ω, which allows one to perform the integration over ω leading to

$$\Delta F_{\mathrm{exc}}^{(2)}=\Delta F_{\mathrm{exc}}^{(3)}.\tag{3.13}$$

In the following paragraph we examine the remaining term $\Delta F_{\mathrm{exc}}^{(1)}$ for the case of a homogeneously magnetized *fluid*, for which $\hat{\rho}(\mathbf{r},\omega)=\rho_0\alpha(\omega)$ so that we can resort to the results of Ref. [9]. There we have analyzed thoroughly the quantity Ω_{int} [Eq. (2.10) in Ref. [9]] which has a completely analogous form. (In particular, the kernel of Ω_{int} has exactly the same long-ranged part.) Thus we have for a ferromagnetic liquid in a sample with vanishing demagnetization factor

$$\Delta F_{\mathrm{exc}}^{(1)}=\Delta F_{\mathrm{exc}}^{(1,\mathrm{SR})}+\Delta F_{\mathrm{exc}}^{(1,\mathrm{LR})}\tag{3.14}$$

with

$$\lim_{V\to\infty}\frac{\Delta F_{\mathrm{exc}}^{(1,\mathrm{SR})}}{V}=\rho^2\sum_{l=0}^{\infty}\widetilde{u}_l\alpha_l^2\quad(\text{fluid phases}),\tag{3.15a}$$

$$\lim_{V\to\infty}\frac{\Delta F_{\mathrm{exc}}^{(1,\mathrm{LR})}}{V}=-\frac{8\pi}{27}\rho^2m^2\alpha_1^2\quad(\text{fluid phases}),\tag{3.15b}$$

where the coefficients $\widetilde{u}_l$ are given by

$$\widetilde{u}_l=\frac{(-1)^l}{\sqrt{\pi}(2l+1)^{3/2}}\int_{\sigma}^{\infty}drr^2\widetilde{w}_{ll0}(r).\tag{3.16}$$

Compared to Ref. [9] the occurrence of $\widetilde{w}_{ll0}(r)$ instead of $-(1/\beta)\widetilde{f}_{ll0}(r)$ together with the different approximation for the homogeneous liquid [Eq. (3.4)] lead to minor quantitative modifications of the liquid phase diagrams, whereas the qualitative features remain unchanged.

Now we return to the discussion of the solid phase. With Eqs. (2.12), (3.7), and $Y_{l0}(\omega)=\sqrt{(2l+1)/(4\pi)}P_l(\cos\theta)$ one obtains

$$\begin{aligned}\Delta F_{\mathrm{exc}}^{(1)}&=\frac{1}{2}\int_V d^3r\int_V d^3r'\rho(\mathbf{r})\rho(\mathbf{r}')\\&\quad\times\sum_{l_1l_2l}w_{l_1l_2l}(r_{12})K_{l_1l_2l}\alpha_{l_1}\alpha_{l_2}P_l(\cos\theta_{12})\end{aligned}\tag{3.17}$$

with

$$K_{l_1l_2l}=\left(\frac{1}{2\pi}\right)^2\sqrt{\frac{4\pi(2l+1)}{(2l_1+1)(2l_2+1)}}C(l_1l_2l,000).\tag{3.18}$$

For the short-ranged contribution the spatial integrations can be extended over the whole space. After performing the transformation $(\frac{1}{2}(\mathbf{r}+\mathbf{r}'),\mathbf{r}-\mathbf{r}')=(\mathbf{r}_S,\mathbf{r}_{12})$ and inserting Eq. (2.9) the integration over $\mathbf{r}_S$ results in

$$\begin{aligned}\Delta F_{\mathrm{exc}}^{(1,\mathrm{SR})}&=\frac{1}{2}\left(\frac{\gamma}{2\pi}\right)^{3/2}\sum_{l_1l_2l}K_{l_1l_2l}\alpha_{l_1}\alpha_{l_2}\sum_{\mathbf{R},\mathbf{R}'\in V}\int_{\mathbb{R}^3}d^3r_{12}\\&\quad\times e^{-\gamma/2[\mathbf{r}_{12}-(\mathbf{R}-\mathbf{R}')]^2}w_{l_1l_2l}^{(\mathrm{SR})}(r_{12})P_l(\cos\theta_{12}).\end{aligned}\tag{3.19}$$

Since the integrand depends only on the difference of the lattice vectors one summation can be carried out:

$$\begin{aligned}\lim_{V\to\infty}\frac{\Delta F_{\mathrm{exc}}^{(1,\mathrm{SR})}}{V}&=\frac{1}{2}\rho_0\left(\frac{\gamma}{2\pi}\right)^{3/2}\sum_{l_1l_2l}K_{l_1l_2l}\alpha_{l_1}\alpha_{l_2}\sum_{\mathbf{R}\in\mathbb{R}^3}\int_{\mathbb{R}^3}d^3r_{12}\\&\quad\times e^{-\gamma/2(\mathbf{r}_{12}-\mathbf{R})^2}w_{l_1l_2l}^{(\mathrm{SR})}(r_{12})P_l(\cos\theta_{12}).\end{aligned}\tag{3.20}$$

Now we express the angle θ_{12} between the direction of the magnetization $\hat{\mathbf{M}}$ and the vector $\mathbf{r}_{12}$ in terms of the solid angles ω_M and ω_r of the directions $\hat{\mathbf{M}}$ and $\hat{\mathbf{r}}_{12}$ in a frame of reference whose polar axis is parallel to the lattice vector $\mathbf{R}$:

$$P_l(\cos\theta_{12})=\frac{4\pi}{2l+1}\sum_m Y_{lm}^*(\omega_M)Y_{lm}(\omega_r).\tag{3.21}$$

Since the exponential factor in Eq. (3.20) depends only on the angle between $\mathbf{r}_{12}$ and $\mathbf{R}$, i.e., on the polar angle θ_r in ω_r, we need to consider only the term $m=0$, and therefore

$$\lim_{V\to\infty}\frac{\Delta F_{\mathrm{exc}}^{(1,\mathrm{SR})}}{V}=\sum_{l_1l_2l}a_{l_1l_2l}\alpha_{l_1}\alpha_{l_2}\tag{3.22}$$

with

$$a_{l_1 l_2 l}=\frac{1}{2}\rho_0\left(\frac{\gamma}{2\pi}\right)^{3/2}K_{l_1 l_2 l}\sum_{\mathbf{R}\in\mathbb{R}^3}P_l(\cos\theta_M)\times\int_{\mathbb{R}^3}d^3r e^{-\gamma/2(\mathbf{r}-\mathbf{R})^2}w^{(\mathrm{SR})}_{l_1 l_2 l}(r)P_l(\cos\theta_r). \tag{3.23}$$

In order to limit the number of terms in Eq. (3.23), the exponential in Eq. (3.6) is expanded and only contributions up to order m^4 are taken into account, i.e.,

$$\tilde{w}^{(\mathrm{SR})}(\mathbf{r},\omega,\omega')=\Phi_a(r)-\frac{1}{2}\beta w^2_{\mathrm{dip}}(\mathbf{r},\omega,\omega')+O(m^6) \tag{3.24}$$

with

$$\Phi_a(r)=\begin{cases} w_{\mathrm{LJ}}(r), & r>R_2 \\ -\epsilon, & R_1<r<R_2 \\ 0, & r<R_1. \end{cases} \tag{3.25}$$

In this approximation the coefficients $\tilde{w}_{l_1 l_2 l}$ can easily be determined from Eq. (3.9) and the product rule for the rotational invariants (see Appendix B of Ref. [9]), which allows one to write Φ^2_{112} as a sum of the invariants $\Phi_{l_1 l_2 l}$. In this order the only nonzero coefficients are

$$w_{000}(r)=(4\pi)^{3/2}\left(\Phi_a(r)-\frac{1}{3}\frac{\beta m^4}{r^6}\right), \tag{3.26}$$

$$w_{022}(r)=w_{202}(r)=-\frac{1}{15}\frac{\beta m^4}{r^6}(4\pi)^{3/2}, \tag{3.27}$$

$$w_{220}(r)=-\frac{1}{15\sqrt{5}}\frac{\beta m^4}{r^6}(4\pi)^{3/2}, \tag{3.28}$$

$$w_{222}(r)=-\frac{1}{15}\sqrt{\frac{2}{35}}\frac{\beta m^4}{r^6}(4\pi)^{3/2}, \tag{3.29}$$

$$w_{224}(r)=-\frac{2}{5}\sqrt{\frac{2}{35}}\frac{\beta m^4}{r^6}(4\pi)^{3/2}. \tag{3.30}$$

C. Lattice sums

Since the integral in Eq. (3.23) depends only on the absolute value of the lattice vector $\mathbf{R}$, one can group the lattice vectors into shells with fixed $|\mathbf{R}|$ and thus consider the restricted sum $\Sigma'_{\mathbf{R}}P_l(\cos\theta_M)=\Sigma_{\mathrm{shell}}P_l(\cos\theta_M)$ over an individual shell first. For $l=0$ this equals the number of vectors belonging to this shell. If we restrain ourselves to cubic lattices using an orthogonal coordinate system which is fixed with respect to this lattice, the vectors within one shell are given by

$$\mathbf{R}=A(\pm n_{\pi(1)},\pm n_{\pi(2)},\pm n_{\pi(3)}), \tag{3.31}$$

where π runs over all six permutations of the numbers $\{1,2,3\}$. The signs vary independently and $\{n_1,n_2,n_3\}$ is a set of integers characterizing the shell. (For an fcc lattice $n_1+n_2+n_3$ must be even, but this is not essential for the following arguments. The result is valid for any cubic lattice.) If some of the numbers n_i are equal or zero not all of the 48 vectors generated by the permutations and sign changes in Eq. (3.31) are different. Thus the result after summing over these 48 vectors has to be divided by an appropiate combinatorial factor. The angle θ_M between $\mathbf{M}$ and $\mathbf{R}$ is

$$\cos\theta_M=\frac{\Sigma_i\pm n_{\pi(i)}M_i}{(\Sigma_i M_i^2\Sigma_i n_i^2)^{1/2}}. \tag{3.32}$$

Therefore one has

$$\sum_{\mathrm{shell}}P_2(\cos\theta_M)=\frac{1}{2}\sum_{\mathrm{signs}}\sum_{\pi}\frac{3(\Sigma_i\pm n_{\pi(i)}M_i)^2-\Sigma_i n^2_{\pi(i)}\Sigma_i M_i^2}{\Sigma_i n_i^2\Sigma_i M_i^2}=\frac{4}{\Sigma_i n_i^2\Sigma_i M_i^2}\sum_{\pi}\left(3\sum_i M_i^2 n^2_{\pi(i)}-\sum_i M_i^2\sum_j n^2_{\pi(j)}\right) \tag{3.33}$$

because the terms $n_{\pi(i)}n_{\pi(j)}$ with $i\neq j$ vanish after summation over the signs. Interchanging the order of the summations yields

$$\sum_{\mathrm{shell}}P_2(\cos\theta_M)=\frac{4}{\Sigma_i n_i^2\Sigma_i M_i^2}\sum_i M_i^2\sum_{\pi}\left(3n^2_{\pi(i)}-\sum_j n^2_{\pi(j)}\right)=0 \tag{3.34}$$

because $\Sigma_\pi 3n^2_{\pi(i)}=\Sigma_\pi\Sigma_j n^2_{\pi(j)}=6(n_1^2+n_2^2+n_3^2)$. [See also the Appendix of Ref. [33] where this result has been derived for the special case $\hat{\mathbf{M}}\|\langle 100\rangle$.] This means that all coefficients $a_{l_1 l_2 l}$ in Eq. (3.23) with $l=2$ are zero. Based on a similar but more lengthy calculation one obtains for $l=4$

$$\sum_{\mathrm{shell}}P_4(\cos\theta)=\frac{7}{12}hz(\mathbf{n})z(\mathbf{M}), \tag{3.35}$$

where h is the number of vectors in the particular shell and

$$z(\mathbf{x}=(x_1,x_2,x_3))=\frac{x_1^4+x_2^4+x_3^4-3(x_1^2x_2^2+x_2^2x_3^2+x_3^2x_1^2)}{|\mathbf{x}|^4}. \tag{3.36}$$

In $O(m^4)$ the term proportional to a_{224} is the only contribution to the free energy which depends on the orientation of $\mathbf{M}$ relative to the lattice. Due to the form of Eq. (3.35) $z(\mathbf{M})$ can be factored out of the summation over $|\mathbf{R}|$ and the most favorable direction of $\mathbf{M}$ is given by the maximum or minimum of $z(\mathbf{M})$ depending on the sign of the remaining lattice sum. The function $z(\mathbf{M})$ attains its maximum for $\mathbf{M}\sim(1,0,0)$ and its minimum for $\mathbf{M}\sim(1,1,1)$ or, respectively, the other directions which result from these under symmetry operations of the cube. For the parameter values which we have considered, the direction $\langle 111\rangle$ parallel to the space diagonal of the cubic unit cell turned out to be the most stable one. This means, e.g., that a solid sphere surrounded by a perfect conductor suppressing the depolarization field should spontaneously choose one of the eight

equivalent ⟨111⟩ directions as the axis of polarization when cooled down from the nonmagnetic phase.

D. Long-ranged contribution for the solid phase

For the long-ranged contribution to the excess free energy [see Eq. (3.10)]

$$\Delta F_{\rm exc}^{\rm (LR)}=-\frac{4}{9}m^2\alpha_1^2\int_V d^3r\int_V d^3r'\,\rho(\mathbf{r})\rho(\mathbf{r}')r_{12}^{-3}\times\Theta(r_{12}-\sigma)P_2(\cos\theta_{12}) \tag{3.37}$$

the thermodynamic limit has to be performed carefully by first considering a finite volume and then increasing its size to infinity for a fixed shape. As for the ferromagnetic liquid one expects that the result will depend on the shape of the volume. For this purpose the density ansatz in Eq. (2.9) is written as a Fourier series

$$\rho(\mathbf{r})=\sum_{\mathbf{q}}\rho_{\mathbf{q}}e^{i\mathbf{q}\cdot\mathbf{r}},\quad \rho_{\mathbf{q}}=\rho_0 e^{-q^2/4\gamma}, \tag{3.38}$$

where $\mathbf{q}$ runs over the reciprocal lattice ($2\pi\mathbf{q}\cdot\mathbf{R}\in\mathbb{Z}$). [We recall that even for finite volumes the sums in Eqs. (2.9) and (3.38) run over an infinite lattice and the density is cut off by the integration limits.] Using again the transformation $(\frac{1}{2}(\mathbf{r}+\mathbf{r}'),\mathbf{r}-\mathbf{r}')=(\mathbf{r}_S,\mathbf{r}_{12})$ one finds

$$\Delta F_{\rm exc}^{\rm (LR)}=-\frac{4}{9}m^2\alpha_1^2\sum_{\mathbf{q},\mathbf{q}'}\rho_{\mathbf{q}}\rho_{\mathbf{q}'}\int_{2V}d^3r_{12}r_{12}^{-3}\Theta(r_{12}-\sigma)\times e^{1/2\,i(\mathbf{q}-\mathbf{q}')\cdot\mathbf{r}_{12}}P_2(\cos\theta_{12})\int_{V_S(\mathbf{r}_{12})}d^3r_S e^{i(\mathbf{q}+\mathbf{q}')\cdot\mathbf{r}_S}. \tag{3.39}$$

The integration region $V_S(\mathbf{r}_{12})$ for the center of mass vector $\mathbf{r}_S$ at fixed $\mathbf{r}_{12}$ is in general given by [9] $V_S(\mathbf{r}_{12})=V_+(\mathbf{r}_{12})\cap V_-(\mathbf{r}_{12})$ with

$$V_\pm(\mathbf{r}_{12})=\{\mathbf{r}\pm\tfrac{1}{2}\mathbf{r}_{12}|\mathbf{r}\in V\}. \tag{3.40}$$

We now consider a cuboid with two equal sides of length L and one side of length kL. Then the set $V_S(\mathbf{r}_{12})$ is also a cuboid so that

$$\int_{V_S(\mathbf{r}_{12})}d^3r_S e^{i\mathbf{q}\cdot\mathbf{r}_S}=\int_{(-L+|x_{12}|)/2}^{(L-|x_{12}|)/2}dx_S\int_{(-L+|y_{12}|)/2}^{(L-|y_{12}|)/2}dy_S\times\int_{(-kL+|z_{12}|)/2}^{(kL-|z_{12}|)/2}dz_S e^{i(q_1x_S+q_2y_S+q_3z_S)}. \tag{3.41}$$

After performing the integrations one realizes that only terms with $\mathbf{q}+\mathbf{q}'=0$ contribute to the bulk term in Eq. (3.39). With $\mathbf{x}=\mathbf{r}_{12}/L=(x_1,x_2,x_3)$ and $\widetilde{V}=V/L^3$ one obtains

$$\frac{F_{\rm exc}^{\rm (LR)}}{V}=-\frac{4}{9}\rho_0^2m^2\alpha_1^2\sum_{\mathbf{q}}e^{-q^2/2\gamma}\int_{2\widetilde{V}}d^3x x^{-3}\Theta(x-\sigma/L)\times e^{iL\mathbf{q}\cdot\mathbf{x}}P_2(\cos\theta)(1-x_1)(1-x_2)(1-x_3/k). \tag{3.42}$$

The term $\mathbf{q}=\mathbf{0}$ is the only one that occurs also in the fluid phase. After some algebra one can prove that this expression is [as expected, see Eqs. (3.22)–(3.24) in Ref. [9]] of the form $-(8\pi/9)\rho_0^2m^2\alpha_1^2I_C(k)$ with

$$I_C(k)=\frac{1}{3}+\frac{2}{\pi k}\int_0^1 dx(1-x)\Big[-x+\sqrt{k^2+x^2}+\sqrt{1+x^2}-\sqrt{1+k^2+x^2}+\ln x-\frac{1}{2}\ln(k^2+x^2)-\ln(1+\sqrt{1+x^2})+\ln(1+\sqrt{1+k^2+x^2})\Big] \tag{3.43}$$

and $I_C(k\to\infty)=1/3$. It is this contribution which has been overlooked by Smithline *et al.* [33] leading them to the wrong conclusion that a ferromagnetic fcc solid cannot be stable. It should be emphasized that for finite aspect ratios k we expect to obtain the same free energy as in the limit $k\to\infty$ if domain formation is taken into account [26,25]. However, a rigorous proof of this statement for a solid within our theory is beyond the scope of this work. For all other terms ($\mathbf{q}\neq0$) in Eq. (3.42) we insert the Rayleigh expansion

$$e^{i\mathbf{q}\cdot\mathbf{r}}=4\pi\sum_{l,m}i^l j_l(qr)Y_{lm}^*(\omega_q)Y_{lm}(\omega_r). \tag{3.44}$$

The coefficients j_l denote spherical Bessel functions which are bounded as $|j_l(x)|\leq M_l/|x|$ with numbers M_l. Thus we deduce for the radial integral in Eq. (3.42)

$$\left|\int_{\sigma/L}^{g(\omega)}dx x^{-1}j_l(Lqx)x^n\right|\leq\frac{M_l}{Lq}\int_{\sigma/L}^{g(\omega)}dx x^{n-2}\to0 \quad \text{for } L\to\infty \text{ and } n\geq1; \tag{3.45}$$

the function $g(\omega)$ defines the upper limit for the radial integration in the direction ω and is determined by the shape of $\widetilde{V}$. For this reason the last three factors in Eq. (3.42) can be replaced by one. In order to determine the bulk contribution of $F_{\rm exc}^{\rm (LR)}/V$ in the thermodynamic limit the integration in Eq. (3.42) can be replaced by an integration over the unit sphere. The neglected parts from the ''corners'' of the cuboid $2\widetilde{V}$ are the Fourier transform of an absolutely integrable function and thus vanish in the limit $Lq\to\infty$. By using Eq. (3.44) and due to the identity $\int dx j_2(x)/x=-j_1(x)/x$ we therefore obtain for the long-ranged contribution

$$\lim_{V\to\infty}\frac{\Delta F_{\rm exc}^{\rm (LR)}}{V}=-\frac{8\pi}{27}\rho_0^2m^2\alpha_1^2\Big(1-6\sum_{\mathbf{q}\neq0}P_2(\cos\theta_q)\times e^{-q^2/2\gamma}\frac{j_1(q\sigma)}{q\sigma}\Big). \tag{3.46}$$

Since, as shown above, for cubic lattices the sum $\Sigma_{\text{shell}} P_2(\cos\theta_q)$ vanishes, in this case the long-ranged part in the limit $k \to \infty$ reduces to the expression given in Eq. (3.15b) for the liquid phase.

In sum these results enable us to calculate the free energy of the solid phase as a function of ρ_0, γ [Eq. (2.9)] and $\{\alpha_l\}$ [Eq. (2.12)] according to [see Eqs. (3.3), (3.10), and (3.13)]

$$F(\rho_0, T; \gamma, \{\alpha_l\}) = F_{\text{ref}} + F_{\text{exc},l} + \Delta F_{\text{exc}}^{(1,\text{SR})} + \Delta F_{\text{exc}}^{(1,\text{LR})} - \Delta F_{\text{exc}}^{(3)}, \tag{3.47}$$

where the different contributions are given by Eqs. (2.5), (3.4), (3.22), (3.46) [recall that $\Delta F_{\text{exc}}^{(1,\text{LR})}$ for the fcc solid happens to be given by Eq. (3.15b)], and (3.11).

IV. PHASE DIAGRAMS AND LINDEMANN PARAMETER

By numerical minimization of Eq. (3.47) and its counterpart for fluid phases with respect to the width parameter γ and the orientational distribution $\alpha(\cos\theta)$ we determine the free energy of the system as a function of the mean density ρ_0:

$$\begin{aligned} F(\rho_0, T) &= \min_{\gamma, \alpha_l} F(\rho_0, T; \gamma, \{\alpha_l\}) \\ &= F(\rho_0, T; \gamma_{\min}(\rho_0, T), \{\alpha_l^{\min}(\rho_0, T)\}). \end{aligned} \tag{4.1}$$

The coexistence densities ρ_1 and ρ_2 of two phases follow from the double tangent construction:

$$\left.\frac{\partial F}{\partial \rho_0}\right|_{\rho_1} = \left.\frac{\partial F}{\partial \rho_0}\right|_{\rho_2}, \quad F(\rho_1) - \rho_1 \left.\frac{\partial F}{\partial \rho_0}\right|_{\rho_1} = F(\rho_2) - \rho_2 \left.\frac{\partial F}{\partial \rho_0}\right|_{\rho_2}. \tag{4.2}$$

Since for the solid phase the numerical determination of $F(\rho_0, T)$ for one value of the parameters ρ_0 and T requires already a substantial CPU time, we have calculated this function for each T only for seven values of ρ_0 within a density interval in which the phase transition is expected. These results are then interpolated with a Chebychev polynomial for which Eq. (4.2) is solved. This procedure also avoids difficulties as far as the numerical differentation with respect to ρ_0 is concerned.

Figure 1 displays the resulting phase diagram for the reduced dipole moment $m^* = m/\sqrt{\sigma^3 \epsilon} = 1$. At low densities there is a wide coexistence region between the isotropic gas and liquid with a critical point at $T_c^* = 1.429$ and $\rho_c^* = 0.296$. At higher densities we find the liquid-solid transition with a density gap $\rho_s^* - \rho_l^* = 0.1$–$0.15$. The dashed line indicates continuous phase transtions between isotropic and ferromagnetic phases. It is terminated by critical end points at the coexistence lines of the first-order transitions. Within the solid phase the dashed line corresponds to the line of Curie points at which the ferromagnetic solid turns into a solid without orientational order (plastic solid), whereas within the liquid phase the line denotes the transition between the isotropic and the ferromagnetic liquid. This line of critical points $\rho_{fc}(T)$ can be obtained analytically from the coefficient of α_1^2 in the excess free energy [see Eq. (7.10) in Ref. [9]]. In the approximation used here, i.e., taking into account only terms up to order m^4 in F_{exc}, this coefficient is fully determined by the long-ranged contributions, which are identical for the liquid and solid phases, so that one finds

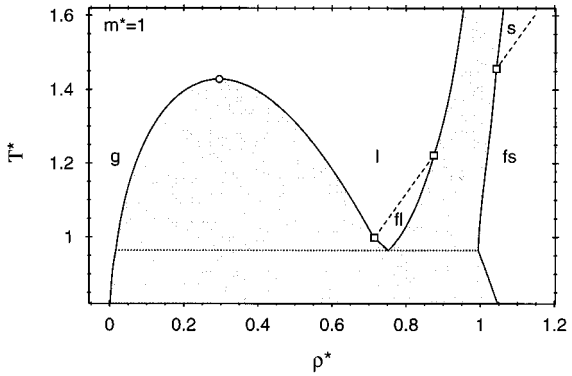

FIG. 1. The phase diagram in terms of $T^* = k_B T/\epsilon$ and $\rho^* = \rho\sigma^3$ for $m^* = m/\sqrt{\sigma^3\epsilon} = 1$ comprises five phases: gas (g), isotropic liquid (l), ferromagnetic liquid (fl), isotropic (plastic), solid (s), ferromagnetic solid (fs). In the shaded area one has two-phase coexistence. The dashed lines indicate second-order phase transitions between orientationally ordered and disordered phases. The circle marks the liquid-gas critical point $(T_c^*, \rho_c^*) = (1.429, 0.296)$ and the squares critical end points: $(T_{cep}^*, \rho_{cep}^*) = (0.998, 0.715)$, (1.222,0.875), and (1.457,1.044). Below the triple point (dotted line) $(T_t^*, \rho_{gt}^*, \rho_{flt}^*, \rho_{fst}^*) = (0.964, 0.017, 0.753, 0.994)$ the system phase separates into the gas phase and the ferromagnetic solid.

$$\rho_{fc}(T) = \frac{9 k_B T}{4\pi m^2}. \tag{4.3}$$

In Ref. [9] it has been demonstrated that the inclusion of higher order terms in m^2 leads only to slight deviations from the straight line given by Eq. (4.3). At the triple temperature $T_t^* = 0.964$ there is three-phase coexistence between the gas phase, the ferromagnetic liquid, and the ferromagnetic solid.

The corresponding phase diagram for $m^* = 1.35$ is shown in Fig. 2. In the temperature interval $T^* = 1.3$–1.8 for the liquid phases we find the features already discussed in Refs.

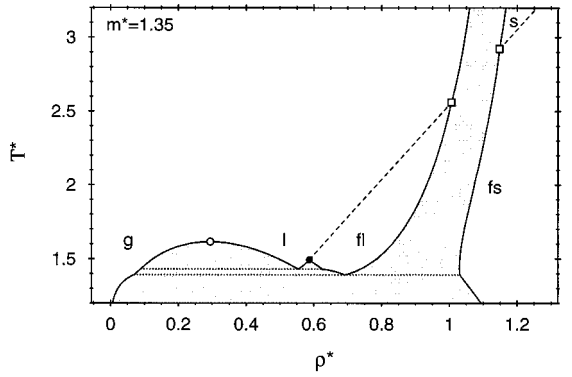

FIG. 2. Phase diagram for $m^* = 1.35$. We use the same designation of the phases and the same notation as in Fig. 1. We find the liquid-gas critical point (open circle) $(T_c^*, \rho_c^*) = (1.615, 0.294)$, the tricritical point (full circle) $(T_{tc}^*, \rho_{tc}^*) = (1.493, 0.587)$, and the two triple points (dotted lines) $(T_{t1}^*, \rho_{gt1}^*, \rho_{lt1}^*, \rho_{flt1}^*) = (1.430, 0.089, 0.553, 0.626)$ and $(T_{t2}^*, \rho_{gt2}^*, \rho_{flt2}^*, \rho_{fst2}^*) = (1.392, 0.070, 0.692, 1.031)$.

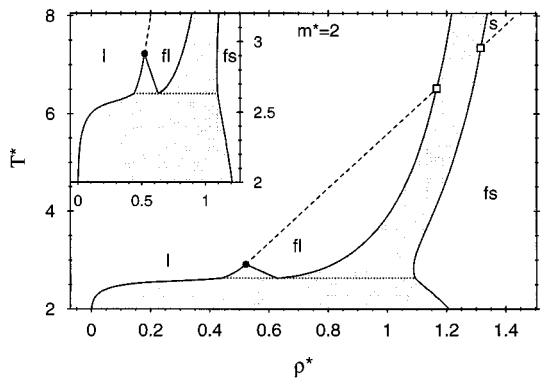

FIG. 3. Phase diagram for $m^*=2$. As compared with Figs. 1 and 2 the liquid-gas critical point has disappeared so that there are only four phases. The plastic solid without orientational order is stable only at very high temperatures and densities. (The closest packing of spheres corresponds to $\rho^*=\sqrt{2}$.) The inset is focused on the tricritical point $(T^*_{tc},\rho^*_{tc})=(2.914,0.522)$ and the triple point $(T^*_t,\rho^*_{lt},\rho^*_{flt},\rho^*_{fst})=(2.633,0.440,0.628,1.095)$.

[8,9], namely, the common critical point between the isotropic gas and the isotropic liquid and a tricritical point. At the latter the character of the isotropic-ferromagnetic liquid phase transition changes from first order to second order. The line of critical points for this transition originates from this tricritical point and ends at a critical end point. In addition there is the ferromagnetic solid at high densities so that two triple points emerge, which in this case are close to each other. (The gas and the ferromagnetic liquid and solid coexist at $T^*=1.392$, the gas and the isotropic and ferromagnetic liquid at $T^*=1.430$.) At high temperatures the solid loses its orientational order along a line of critical points. The same is true for the case $m^*=2$ (Fig. 3) in which the liquid-gas critical point has disappeared and only a single isotropic fluid phase is left within our present approximation. The region of stability of the ferromagnetic liquid increases substantially with increasing dipole moment. Only for small dipole moments $m^*<1$ is the ferromagnetic liquid preempted completely by the freezing transition as shown in Fig. 4 for $m^*=0.85$. At even lower values of the dipole moment the

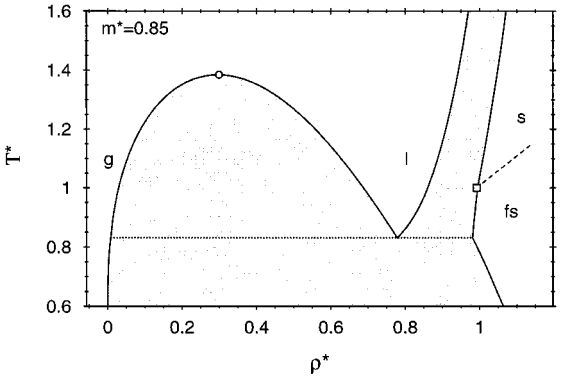

FIG. 4. Phase diagram for $m^*=0.85$. For this small dipole moment the ferromagnetic liquid phase is never stable. The liquid-gas critical point is given by $(T^*_c,\rho^*_c)=(1.385,0.299)$, the triple point by $(T^*_t,\rho^*_{gt},\rho^*_{lt},\rho^*_{fst})=(0.831,0.0081,0.779,0.981)$, and the critical end point by $(T^*_{cep},\rho^*_{cep})=(1.004,0.995)$.

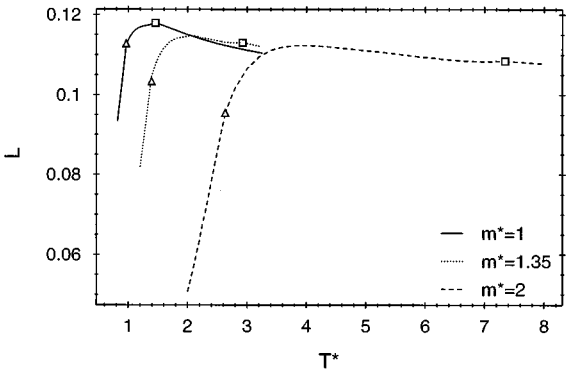

FIG. 5. Temperature dependence of the Lindemann parameter along the gas-solid and gas-liquid coexistence lines for three values of the dipole moment. The triple points are denoted by triangles and the critical end points by squares.

critical end point temperature falls below the triple point temperature.

Hemmer and Imbro [19] have analyzed the Heisenberg fluid in the limit of very weak but long-ranged interactions for which the mean-field theory turns out to be exact. It is interesting to note that they have found a qualitatively identical sequence of phase diagrams.

Usually the width of the thermal vibrations of the particles around their equilibrium positions is not measured in terms of γ but by the Lindemann parameter L, which is the root mean square displacement of the particles from their equilibrium positions normalized to the nearest neighbor distance $R_{\rm nn}$. Here we approximate L by

$$L=R_{\rm nn}^{-1}\left[\left(\frac{\gamma}{\pi}\right)^{3/2}\int_{\mathbb{R}^3}d^3r r^2 e^{-\gamma r^2}\right]^{1/2} \tag{4.4}$$

which yields $L=2^{-2/3}3^{1/2}\rho_0^{1/3}\gamma^{1/2}$ for the fcc lattice. Figure 5 displays the temperature dependence of the Lindemann parameter along the gas-solid and liquid-solid coexistence lines for three values of the dipole moment. Below and slightly above the triple point L increases with temperature while at higher temperatures it gradually levels off at an approximately constant value independent of m^* as expected from the phenomenological Lindemann criterium [48]. At the critical end points the Lindemann parameter exhibits a small upward cusp.

V. BODY-CENTERED-TETRAGONAL SOLID

Wei and Patey have observed a body-centered-tetragonal (bct) lattice for the ferromagnetic solid in a Monte Carlo simulation of dipolar soft spheres [2]. Weis and Levesque [4] examined both the bct and the fcc structure in a simulation of dipolar hard spheres, but they were not able to decide which one is more stable. They report a helical variation of the local magnetization in the fcc crystal. This possibility is not yet taken into account in our calculations [see the assumption (i) in Sec. II] in order to avoid in this first step of our analysis the enormously increased complexity induced by a spatially varying orientational distribution (see, e.g., Ref. [25]). Moreover it cannot be ruled out that this observation is an artefact due to the periodic boundary conditions used in the simula-

tions. The bct structure has also been identified as the ground state of an electrorheological fluid [49] even if higher multipole moments are taken into account [50]. This has been confirmed experimentally [36]. Inspired by these findings we have examined the stability of the bct solid within the framework of the density-functional theory developed in Secs. II and III.

In this case the lattice vectors are given by

$$\mathbf{R}=\frac{R_1}{2}(\sqrt{6}n_1,\sqrt{6}n_2,2n_3), \tag{5.1}$$

where all three numbers $n_i \in \mathbb{Z}$ have the same parity. The nearest neighbor distance is given by $2R_1=2(1/6\rho_0)^{1/3}$ and the magnetization points into the z direction. The corresponding reciprocal lattice vectors are

$$\mathbf{q}=\frac{2\pi}{R_1}(m_1/\sqrt{6},m_2/\sqrt{6},m_3/2) \tag{5.2}$$

with $m_i \in \mathbb{Z}$ and $m_1+m_2+m_3$ even. In contrast to the cubic lattice the relation $\Sigma_{\text{shell}}P_2(\cos\theta_M)=0$ does not hold; in fact

$$\cos^2\theta_M=\frac{4n_3^2}{6(n_1^2+n_2^2)+4n_3^2} \tag{5.3}$$

and thus $P_2(\cos\theta_M)$ is constant within each shell, which as above is defined by $|\mathbf{R}|=\text{const}$. (Here one shell consists of only up to 16 elements.) Therefore the contributions with $l=2$ in Eq. (3.22) and the sum in Eq. (3.46) do not vanish for the bct lattice.

If these changes are taken into account the free energy of the bct solid can be calculated in the same way as for the fcc solid using Eq. (3.47) and the equations referenced there. Again this function is minimized with respect to the width parameter γ and the orientational distributions coefficients α_l for fixed mean density ρ_0. The comparison of the numerical results for $F_{\text{bct}}(\rho_0)$ and $F_{\text{fcc}}(\rho_0)$ reveals that within our approximation the bct structure is *less* stable than the fcc structure for all considered values of the parameters ($m^* \leqslant 2$) and therefore the phase diagrams do not contain phase transitions between different solid structures.

VI. SUMMARY

We have analyzed the phase behavior of Stockmayer fluids by using a suitably generalized modified weighted density approximation for the density-functional theory. The following main results have been obtained.

(i) For small dipole moments the phase diagram resembles that of the Lennard-Jones fluid with a critical point and a triple point. Within the solid phase there are second-order phase transitions along a line of Curie points between an orientationally disordered solid and a ferromagnetic solid (Fig. 4). In the latter phase the magnetization points along the $\langle 111\rangle$ direction of the fcc lattice.

(ii) For larger dipole moments a ferromagnetic nematic phase appears between a line of critical points and the freezing transition (Fig. 1). This line is given by Eq. (4.3) and is terminated by two critical end points on the gas-liquid and the liquid-solid coexistence line, respectively.

(iii) Upon a further increase of the dipole moment the isotropic-ferromagnetic liquid transition turns first order within a temperature interval determined by an emerging second triple point and a tricritical point (Fig. 2).

(iv) For even larger dipole moments the isotropic gas-liquid transition disappears due to the formation of a ferromagnetic liquid at high temperatures (Fig. 3). The orientationally disordered solid is stable only at very high temperatures.

(v) The Lindemann parameter L, which measures the mean amplitude of the thermal vibrations of the particles in the solid phases, is approximately constant ($L=0.11$–0.12) along the freezing line but decreases near the triple point and along the sublimation line (Fig. 5). L exhibits a small cusp singularity at the critical end points.

(vi) Within our approximation the body-centered-tetragonal lattice is less stable than the fcc lattice.

[1] D. Wei and G.N. Patey, Phys. Rev. Lett. **68**, 2043 (1992).
[2] D. Wei and G.N. Patey, Phys. Rev. A **46**, 7783 (1992).
[3] J.J. Weis, D. Levesque, and G.J. Zarragoicoechea, Phys. Rev. Lett. **69**, 913 (1992).
[4] J.J. Weis and D. Levesque, Phys. Rev. E **48**, 3728 (1993).
[5] M.J. Stevens and G.S. Grest, Phys. Rev. E **51**, 5962 (1995).
[6] M.J. Stevens and G.S. Grest, Phys. Rev. E **51**, 5976 (1995).
[7] D. Wei, G.N. Patey, and A. Perera, Phys. Rev. E **47**, 506 (1993).
[8] B. Groh and S. Dietrich, Phys. Rev. Lett. **72**, 2422 (1994); **74**, 2617 (1995).
[9] B. Groh and S. Dietrich, Phys. Rev. E **50**, 3814 (1994).
[10] K. Sano and M. Doi, J. Phys. Soc. Jpn. **52**, 2810 (1983).
[11] M. Widom and H. Zhang, in *Complex Fluids*, edited by E. Sirota, D. Weitz, T. Witten, and J.N. Israelachvili, MRS Symposia Proceedings No. 248 (Materials Research Society, Pittsburgh, 1992), p. 235.
[12] H. Zhang and M. Widom, Phys. Rev. E **49**, R3591 (1994).
[13] H. Zhang and M. Widom, J. Magn. Magn. Mater. **122**, 119 (1993).
[14] P. de Smedt, P. Nielaba, J.L. Lebowitz, J. Talbot, and L. Dooms, Phys. Rev. A **38**, 1381 (1988).
[15] D. Marx, P. Nielaba, and K. Binder, Phys. Rev. Lett. **67**, 3124 (1991).
[16] E. Lomba, J.J. Weis, N.G. Almarza, F. Bresme, and G. Stell, Phys. Rev. E **49**, 5169 (1994).
[17] J.M. Tavares, M.M. Telo da Gama, P.I.C. Teixeira, J.J. Weis, and M.J.P. Nijmeijer, Phys. Rev. E **52**, 1915 (1995).
[18] J.S. Høye and G. Stell, Phys. Rev. Lett. **36**, 1569 (1976).
[19] P.C. Hemmer and D. Imbro, Phys. Rev. A **16**, 380 (1977).
[20] L. Feijoo, C.-W. Woo, and V.T. Rajan, Phys. Rev. B **22**, 2404 (1980).
[21] M.J.P. Nijmeijer and J.J. Weis, Phys. Rev. Lett. **75**, 2887 (1995); Phys. Rev. E **53**, 591 (1996).
[22] G.R. Luckhurst and S. Romano, Proc. R. Soc. London Ser. A **373**, 111 (1980).

[23] M.M. Telo da Gama, Mol. Phys. **52**, 585 (1984).
[24] A. Perera, P.G. Kusalik, and G.N. Patey, Mol. Phys. **60**, 77 (1987).
[25] B. Groh and S. Dietrich, Phys. Rev. E **53**, 2509 (1996).
[26] R.B. Griffiths, Phys. Rev. **176**, 655 (1968).
[27] M. Widom and H. Zhang, Phys. Rev. Lett. **74**, 2616 (1995).
[28] Y. Singh, Phys. Rep. **207**, 351 (1991), and references therein.
[29] W.A. Curtin and N.W. Ashcroft, Phys. Rev. Lett. **56**, 2775 (1986).
[30] U.P. Singh, U. Mohanty, and Y. Singh, Phys. Rev. A **38**, 4377 (1988); Physica A **158**, 817 (1989).
[31] J.F. Marko, Phys. Rev. Lett. **60**, 325 (1988); Phys. Rev. A **39**, 2050 (1989).
[32] M.C. Mohato, R. Lakshmi, R. Pandit, and H.R. Krishnamurthy, Phys. Rev. A **38**, 1049 (1988).
[33] S.J. Smithline, S.W. Rick, and A.D.J. Haymet, J. Chem. Phys. **88**, 2004 (1988).
[34] J.D. McCoy, S. Singer, and D. Chandler, J. Chem. Phys. **87**, 4853 (1987).
[35] W.E. McMullen and D.W. Oxtoby, J. Chem. Phys. **86**, 4146 (1987).
[36] T. Chen, R.N. Zitter, and R. Tao, Phys. Rev. Lett. **68**, 2555 (1992).
[37] T.V. Ramakrishnan and M. Yussouff, Phys. Rev. B **19**, 2775 (1979).
[38] W.E. McMullen and D.W. Oxtoby, J. Chem. Phys. **88**, 1476 (1988).
[39] J.A. Barker and D. Henderson, J. Chem. Phys. **47**, 4714 (1967).
[40] R. Evans, in *Fundamentals of Inhomogeneous Fluids*, edited by D. Henderson (Marcel Dekker, New York, 1992), p. 85.
[41] R. Ohnesorge, dissertation, Universität München, 1994.
[42] A.R. Denton and N.W. Ashcroft, Phys. Rev. A **39**, 4701 (1989).
[43] A. Kyrlidis and R.A. Brown, Phys. Rev. A **44**, 8141 (1991).
[44] N.F. Carnahan and K.E. Starling, J. Chem. Phys. **51**, 635 (1969).
[45] J.P. Hansen and L. Verlet, Phys. Rev. **184**, 151 (1969).
[46] W.R. Smith and D. Henderson, Mol. Phys. **19**, 411 (1970).
[47] C.G. Gray and K.E. Gubbins, *Theory of Molecular Fluids* (Clarendon, Oxford, 1984).
[48] F.A. Lindemann, Phys. Z. **11**, 609 (1910).
[49] R. Tao and J.M. Sun, Phys. Rev. Lett. **67**, 398 (1991).
[50] R. Friedberg and Y.K. Yu, Phys. Rev. B **46**, 6582 (1992).